Determination of quadrupolar dispersion coefficients of the alkali-metal atoms interacting with different material media

Harpreet Kaur,[1] Vipul Badhan,[1] Bindiya Arora,[1,2,*] and B. K. Sahoo[3]
[1]*Department of Physics, Guru Nanak Dev University, Amritsar, Punjab 143005, India*
[2]*Perimeter Institute for Theoretical Physics, Waterloo, Ontario, Canada N2L 2Y5*
[3]*Atomic, Molecular and Optical Physics Division, Physical Research Laboratory, Navrangpura, Ahmedabad 380009, India*

(Received 16 August 2022; accepted 6 October 2022; published 20 October 2022)

In the present work, we determine the C_5 coefficients along with their uncertainties due to quadrupole polarization effects of all the alkali atoms interacting with a metal (Au), a semiconductor (Si), and four dielectric materials (SiO_2, SiN_x, yttrium aluminum garnet, and sapphire). The required dynamic electric quadrupole ($E2$) polarizabilities are evaluated by calculating $E2$ matrix elements of a large number of transitions in the alkali atoms by employing a relativistic coupled-cluster method. A significant contribution towards the long-range van der Waals potential is made by the quadrupole polarization effects. Our finding shows that contributions from the C_5 coefficients to the atom-wall interaction potentials are pronounced at short distances (1–10 nm). The C_3 coefficients of a Fr atom interacting with the above material media are also reported. These results could be useful in understanding the interactions of alkali atoms trapped in different material bodies during high-precision measurements.

DOI: 10.1103/PhysRevA.106.042813

I. INTRODUCTION

Dispersion coefficients due to van der Waals (vdW) interactions between atoms and material walls have attracted significant interest in the last two decades [1] after their numerous applications in physisorption [2,3], storage [4], nanoelectromechanical systems [5], quantum reflection [6], atomic clocks [7], atomic chips [8], atom vapor sensors [9], and so on. The attractive potential between an atom and a wall arises from quantum fluctuations at the zero-contact point due to resonant coupling of virtual photons emitted from the atom with different electromagnetic modes of the surface of the wall [10]. This phenomenon can be described by non-pairwise additive Lifshitz theory [11]. However, often crude approximations have been made in this theory for simplicity by considering only the dipole polarization effects due to their predominant contributions. Following the perturbation-theory analysis, the atom-wall interaction potentials can be expressed as a sum of contributions from multipole-polarizability (i.e., dipole, quadrupole, octupole, etc.) effects of atoms [12].

It has been pointed out that the corrections to the total potential due to multipole polarizations in atom-wall systems must be taken into account in the vicinity of physisorption rendered by the vdW interactions [13]. Liebsch investigated the importance of the quadrupole contributions of atomic properties in the determination of atom-metal attractive interaction potentials and found 5%–10% enhancements in the interaction potentials due to these contributions using the density-functional theory (DFT) [13]. For atoms placed closed to surfaces, some of the selective quadrupole resonances could play pivotal roles in enhancing the atom-surface interaction significantly such that their contributions to the potentials can be higher than the dipole component contributions as noted by Klimov and Ducloy using an analytical analysis [14]. The dispersion coefficients arising from dipole (C_3) and quadrupole (C_5) interactions with the material walls were inspected by Tao and Rappe between different atoms and metal surfaces using the DFT method, and they showed that the C_5 term makes a contribution of about 20% to the long-range part [15]. There are many other works that highlight the importance of higher-order multipole contributions to the atom-wall interaction potentials [16–21], whereas Lach *et al.* [21] have provided a more accurate description of the vdW potentials for the interactions of atoms with the surfaces of perfect conductors and dielectrics materials by taking into account contributions from the dipole, quadrupole, octupole, and hexapole polarizabilities of the atoms within the framework of Lifshitz theory.

In the past decade, alkali atoms have been used to understand the behavior of vdW interactions with different materials using various theoretical and experimental techniques due to their fairly simple electronic configuration [9,22–25]. The Fr atom is being studied keenly for its parity nonconservation effects, in the search for a permanent electron electric dipole moment, and for other high-precision spectroscopy measurements using laser-trapping and -cooling techniques [26–28]. For these applications, measurements are carried out through atom interferometry [29–31]. In atom interferometry, fluctuations are induced due to decoherence coming from surface interactions [32]. It is speculated that these fluctuations might appear stronger for heavy atoms. Hence, the study of Fr material can be considered to be as important as studying other alkali atoms. Although studies

*bindiya.phy@gndu.ac.in

related to C_3 coefficients of Fr with a perfect conductor were carried out earlier [33,34], these coefficients are not available for real material media.

To gain insight into the importance of quadrupole polarizability contributions from alkali atoms to their interaction potential with different material walls, we have evaluated the vdW dispersion coefficients arising due to the dipole term (C_3) and next-higher-order quadrupole term (C_5) for all alkali-metal atoms with different materials, including metals, semiconductors, and dielectrics over an arbitrary range of separation distance. Our work is in agreement with previous studies that indicated the dominance of quadrupole polarization effects evaluated using other methods [13–15]. Particularly, we have probed the range of separation distance for which quadrupole effects are more significant. The C_3 and C_5 coefficients depend upon the polarizabilities of atoms and the permittivity of the material walls at imaginary frequencies. The accuracy of these coefficients can be achieved by using the appropriate methods to calculate these properties. We have used a relativistic all-order (AO) method to calculate the polarizabilities of the alkali atoms, and the Kramers-Kronig relation is used to determine the permittivity of materials at imaginary frequencies. Using these vdW coefficients, we have computed and investigated the potential curves for the considered atom-wall systems.

In the following section, we provide a brief theory related to the interaction potential at arbitrary separation. Then we provide the method to evaluate the required properties of the materials and atom and an evaluation of the uncertainty in the dispersion coefficients in Sec. III and the results and discussion in Sec. IV. Finally, we conclude our work in Sec. V. Unless stated otherwise, atomic units (a.u.) are used throughout.

II. THEORY

The exact theory for the calculation of the vdW interaction potential between an atom and the material surface was given in Ref. [21]. Here, we give only a brief outline of the expressions for the atom-wall vdW interaction potentials due to multipole dispersion coefficients. The general expression for the total attractive interaction potential $U_{\rm total}$ arising from the fluctuating multipole moments of an atom interacting with its image on the surface is given by [20]

$$U_{\rm total}(z) = U_d(z) + U_q(z) + \cdots, \tag{1}$$

where U_d, U_q, and so on are the contributions from the dipole, quadrupole, etc., and z is the separation distance between the atom and wall in nanometers. Due to the predominant nature of the dipole component, often, $U_{\rm total}(z)$ is approximated as $U_d(z)$, but we also estimate contributions from $U_q(z)$ in this work. In terms of the permittivity values of the material and dynamic polarizabilities of the atoms, we can express [21,35,36]

$$U_d(z) = -\frac{\alpha_{\rm fs}^3}{2\pi}\int_0^\infty d\omega\omega^3\alpha_d(\iota\omega) \times \int_1^\infty d\chi\, e^{2\chi\alpha_{\rm fs}\omega z} H(\chi, \epsilon_r(\iota\omega)) \tag{2}$$

and

$$U_q(z) = -\frac{\alpha_{\rm fs}^5}{12\pi}\int_0^\infty d\omega\omega^5\alpha_q(\iota\omega) \times \int_1^\infty d\chi\, e^{2\chi\alpha_{\rm fs}\omega z}(2\chi^2-1)H(\chi, \epsilon_r(\iota\omega)). \tag{3}$$

In the above two expressions, $\alpha_{\rm fs}$ is the fine-structure constant, χ is the Matsubara frequency, and $\alpha_d(\iota\omega)$ and $\alpha_q(\iota\omega)$ are the dynamic dipole and quadrupole polarizabilities of the ground state of the considered atom at imaginary frequencies. The expression for function $H(\chi, \epsilon(\iota\omega))$ is given by [37]

$$H(\chi,\epsilon) = (1-2\chi^2)\frac{\chi' - \epsilon_r\chi}{\chi' + \epsilon_r\chi} + \frac{\chi' - \chi}{\chi' + \chi}, \tag{4}$$

where $\chi' = \sqrt{\chi^2 + \epsilon_r - 1}$ and ϵ_r is the real part of the dynamic permittivity of the material wall at imaginary frequency. Approximating the total potential until quadrupole effects, at short distances ($z \to 0$), the preceding formulas are now given by

$$U_{\rm total}(z) = -\frac{C_3}{z^3} - \frac{C_5}{z^5}, \tag{5}$$

where the C_3 and C_5 coefficients are defined as

$$C_3 = \frac{1}{4\pi}\int_0^\infty d\omega\alpha_d(\iota\omega)\frac{\epsilon_r(\iota\omega)-1}{\epsilon_r(\iota\omega)+1} \tag{6}$$

and

$$C_5 = \frac{1}{4\pi}\int_0^\infty d\omega\alpha_q(\iota\omega)\frac{\epsilon_r(\iota\omega)-1}{\epsilon_r(\iota\omega)+1}. \tag{7}$$

III. METHOD OF EVALUATION

As mentioned in the previous section, the evaluation of the C_3 and C_5 coefficients requires knowledge of $\epsilon_r(\iota\omega)$ and $\alpha(\iota\omega)$ of the material media and atoms, respectively. The real part of the permittivity at imaginary-frequency $\epsilon_r(\iota\omega)$ values cannot be obtained experimentally, but their values can be inferred from the imaginary part of the permittivity at real frequencies using the Kramers-Kronig relations. Similarly, accurate determination of dynamic values of α_d and α_q at imaginary frequencies are challenging in the *ab initio* approach. However, for alkali atoms, these can be evaluated very accurately using the sum-over-states approach. Below, we discuss evaluation procedures for $\epsilon_r(\iota\omega)$ and $\alpha(\iota\omega)$.

A. Dynamic electric permittivity

The imaginary part of the dynamic electric permittivity $\epsilon_i(\omega)$ can be given by

$$\epsilon_i(\omega) = 2n(\omega)\kappa(\omega), \tag{8}$$

where $n(\omega)$ and $\kappa(\omega)$ are the refractive indices and extinction coefficients of the materials at real frequencies, respectively. Discrete $n(\omega)$ and $\kappa(\omega)$ values of the considered material media for a wide range of frequencies are tabulated in the *Handbook on Optical Constants of Solids* by Palik [38].

Using these values, we have extrapolated values of $\epsilon_i(\omega)$ for continuous frequencies for a large range. Now using the Kramers-Kronig relation, we can express the real part of dynamic permittivities $\epsilon_r(\iota\omega)$ at imaginary frequencies such that

$$\epsilon_r(\iota\omega) = 1 + \frac{2}{\pi}\int_0^\infty d\omega' \frac{\omega'\epsilon_i(\omega')}{\omega^2 + \omega'^2}. \tag{9}$$

For the case of the semiconductor (Si) and dielectrics [SiO_2, yttrium aluminum garnet (YAG), ordinary sapphire (OS), and extraordinary sapphire (ES)], we have used optical constants ranging from 0.1 to 10000 eV from Palik [38]. For the case of Au, the ϵ values at very small energies are very significant; hence, in addition to the experimental values from Ref. [38], we have extrapolated the values of real permittivity at imaginary frequencies using the Drude model for metals as

$$\epsilon_r(\iota\omega) = 1 - \frac{\omega_p^2}{\omega(\omega + \iota\gamma)}, \tag{10}$$

where ω_p is the plasma frequency and γ is the relaxation frequency. We have used $\omega_p = 9.0\,\text{eV}$ and $\gamma = 0.035\,\text{eV}$ as in [36,39]. For the case of SiN_x, an amorphous dielectric material, we use the Tauc-Lorentz model for amorphous materials [40] to estimate the electric permittivity at imaginary frequencies, the expression of which is given as

$$\epsilon_r(\iota\omega) = \frac{\omega^2 + (1 + g_0)\omega_0^2}{\omega^2 + (1 - g_0)\omega_0^2}, \tag{11}$$

where the parameters $g_0 = 0.588$ and $\omega_0 = 0.005$ are SiN_x's response functions [40].

B. Dynamic polarizabilities

We already reported $\alpha_d(\iota\omega)$ values for the Li to Cs alkali atoms in our previous works [37,41]. Here, we give $\alpha_d(\iota\omega)$ values for the Fr atom and $\alpha_q(\iota\omega)$ values for all the alkali-metal atoms by evaluating them using the following procedures.

Total electron correlation contributions to $\alpha_d(\iota\omega)$ and $\alpha_q(\iota\omega)$ for atomic states of alkali atoms can be expressed as [42]

$$\alpha_l(\iota\omega) = \alpha_{l,\text{core}}(\iota\omega) + \alpha_{l,\text{vc}}(\iota\omega) + \alpha_{l,\text{val}}(\iota\omega), \tag{12}$$

where $l = d$ corresponds to dipole polarizability and $l = q$ corresponds to quadrupole polarizability. Subscripts core, vc, and val correspond to core, valence-core, and valence contributions to the total polarizability, respectively. In the alkali atoms, $\alpha_{l,\text{val}}(\iota\omega)$ contributes predominantly, followed by $\alpha_{l,\text{core}}(\iota\omega)$, and contributions from $\alpha_{l,\text{vc}}(\iota\omega)$ are negligibly small. These contributions are estimated in the following way.

To begin with, the electronic configuration of alkali atoms is divided into a closed core and a valence orbital in order to obtain the mean-field Dirac-Fock (DF) wave function of the respective closed shell ($|0_c\rangle$) using the DF method. The mean-field wave functions of the atomic states of the alkali atoms are then defined by appending the respective valence orbital v as

$$|\phi_v\rangle = a_v^\dagger|0_c\rangle. \tag{13}$$

Using these mean-field DF wave functions, we calculated the vc contributions to the dipole and quadrupole polarizability using the following formula:

$$\alpha_{l,\text{vc}}(\iota\omega) = \frac{2}{(2L+1)(2J_v+1)} \times \sum_m^{N_c} \frac{(\mathcal{E}_m - \mathcal{E}_v)|\langle\psi_v||\mathbf{O_L}||\psi_m\rangle_{\text{DF}}|^2}{(\mathcal{E}_m - \mathcal{E}_v)^2 + \omega^2}, \tag{14}$$

where J_v corresponds to the total angular momentum of the state. Similarly, the core contributions can be given by

$$\alpha_{l,\text{core}}(\iota\omega) = \frac{2}{(2L+1)} \times \sum_a^{N_c}\sum_m^{B} \frac{(\mathcal{E}_m - \mathcal{E}_a)|\langle\psi_a||\mathbf{O_L}||\psi_m\rangle|^2}{(\mathcal{E}_m - \mathcal{E}_a)^2 + \omega^2}, \tag{15}$$

where the first sum for core orbitals is restricted from a to total core orbitals N_c, the second sum is restricted by involving intermediate states m up to allowed bound states B using the respective dipole and quadrupole selection rules, $L = 1$ and $\mathbf{O}_1 = \mathbf{D}$ are required for the dipole operator to give α_d, $L = 2$ and $\mathbf{O}_2 = \mathbf{Q}$ are required for the quadrupole operator to give α_q, and $\mathcal{E}_i$ is the DF energy of the state. We have adopted the random-phase approximation (RPA) to evaluate the above expression to account for the core correlations [43].

The major contributions to the total dipole and quadrupole polarizabilities are provided by the valence contributions; Hence, it is important to calculate the valence polarizability using accurate methods. We divide the valence contributions into two parts: main and tail. The main part corresponds to polarizability contributions by the low-lying dominant transitions responsible for very large polarizability contributions. For the evaluation of the main part of the valence contribution of total polarizability, we have employed the AO method to evaluate accurate wave functions. These wave functions $|\psi_v\rangle$, with v denoting the valence orbital, are represented using a singles and doubles (SD) approximation of the AO method as [44]

$$|\psi_v\rangle_{\text{SD}} = \Bigg[1 + \sum_{ma}\rho_{ma}a_m^\dagger a_a + \frac{1}{2}\sum_{mrab}\rho_{mrab}a_m^\dagger a_r^\dagger a_b a_a + \sum_{m\neq v}\rho_{mv}a_m^\dagger a_v + \sum_{mla}\rho_{mrva}a_m^\dagger a_r^\dagger a_a a_v\Bigg]|\phi_v\rangle, \tag{16}$$

where $a^\dagger$ and a represent the second-quantization creation and annihilation operators, respectively, whereas the excitation coefficients are denoted by ρ. The subscripts m, r and a, b refer to the virtual and core orbitals, respectively. ρ_{ma} and ρ_{mv} are the single-excitation coefficients, whereas ρ_{mrab} and ρ_{mrva} are the double-excitation coefficients. To take into account the important experimental contributions these *ab initio* wave functions are modified by changing the valence excitation coefficient with modified ρ_{mv} using the scaling procedure such that

$$\rho'_{mv} = \rho_{mv}\frac{\delta E_v^{\text{expt}}}{\delta E_v^{\text{theory}}}. \tag{17}$$

After obtaining the wave functions of the considered states of alkali-metal atoms using the AO method, we determine the matrix elements, with k being the intermediate state, using the following expression [45]:

$$O_{L,vk} = \frac{\langle\psi_v|\mathbf{O}_L|\psi_k\rangle}{\sqrt{\langle\psi_v|\psi_v\rangle\langle\psi_k|\psi_k\rangle}}, \tag{18}$$

where $O_{L,vk}$ corresponds to either dipole $E1$ or quadrupole $E2$ matrix elements depending on **D** or **Q** operators, respectively. Using these matrix elements, the final expression for the main part of the valence contribution to either the $E1$ or $E2$ polarizability at imaginary frequency is then given as

$$\alpha_{l,\mathrm{Main}}(\iota\omega) = \frac{2}{(2L+1)(2J_v+1)} \times \sum_{m>N_c, m\neq v} \frac{(E_m - E_v)|\langle\psi_v||\mathbf{O}_L||\psi_m\rangle|^2}{(E_m - E_v)^2 + \omega^2}, \tag{19}$$

where the sum is now restricted by entailing the intermediate states m after N_c and up to I. We have considered 10–12 $E1$ and $E2$ matrix elements for the dominant transitions of considered atoms using the AO method. For precise calculations, we use experimental energies E_i from the National Institute of Standards and Technology (NIST) database [46]. Contributions from the remaining high-lying states are referred to as the tail part and are evaluated as

$$\alpha_{l,\mathrm{Tail}}(\iota\omega) = \frac{2}{(2L+1)(2J_n+1)} \times \sum_{m>I} \frac{(\mathcal{E}_m - \mathcal{E}_n)|\langle\psi_n||\mathbf{O}_L||\psi_m\rangle_{\mathrm{DF}}|^2}{(\mathcal{E}_m - \mathcal{E}_n)^2 + \omega^2}, \tag{20}$$

where $m > I$ means that states included in the main contribution evaluation are excluded here. Since the tail contributions are much smaller in comparison to the main part, we calculate them using the DF method.

C. Uncertainty evaluation

The sources of uncertainties in the final values of the dispersion coefficients can be accounted for by the polarizability values of the atoms and the permittivity values of the materials. We have considered the uncertainties in the final values of the dispersion coefficients only from the polarizability calculations of the atoms without accounting for errors from experimental data for the optical constants n and k. To evaluate the uncertainties from the different contributions of polarizabilities, we have adopted procedures given in Ref. [47]. One of the sources of uncertainties to the matrix elements of the SD method can arise from the neglected triple excitations, which can be estimated by considering triple-excitation effects perturbatively in the SD method (SDpT method). Again, *ab initio* values of the SD and SDpT methods can be improved by scaling the excitation amplitudes using the experimental energies. The scaling procedures are explained in Refs. [48,49]. Using these methods, uncertainties of the calculated matrix elements are given as the sum of differences in the values from the SD and SDpT methods and from the *ab initio* and scaled calculations. Uncertainties of the tail, core, and vc contributions of the polarizabilities are estimated using the approach discussed in Ref. [47]. From this procedure, we have assigned a total of 10% and 50% error bars to the core and vc contributions. The final uncertainty of the polarizability value is given by adding the individual uncertainties in the quadrature. From the uncertainties in the polarizability values we have obtained the uncertainties in the dispersion coefficients.

TABLE I. Contributions to the ground-state dipole polarizability (in a.u.) of the Fr atom. Various contributions along with the absolute values of reduced $E1$ matrix elements contributing to the main part of the valence correlations are quoted explicitly. Tail, core, and valence-core contributions are also given. The core contribution is estimated using the RPA method. Uncertainties in the values are given in parentheses. Our final value is compared with previously reported high-precision calculations.

Contribution	$E1$	$\alpha_d(0)$
Main		
$7S_{1/2} - 7P_{1/2}$	4.277(8)[a]	109.4(4)
$7S_{1/2} - 8P_{1/2}$	0.33(3)	0.34(7)
$7S_{1/2} - 9P_{1/2}$	0.11(2)	0.03(1)
$7S_{1/2} - 10P_{1/2}$	0.06(2)	0.008(4)
$7S_{1/2} - 11P_{1/2}$	0.03(1)	0.003(2)
$7S_{1/2} - 12P_{1/2}$	0.024(9)	0.001(1)
$7S_{1/2} - 7P_{3/2}$	5.90(2)[a]	182.8(9)
$7S_{1/2} - 8P_{3/2}$	0.93(5)	2.68(3)
$7S_{1/2} - 9P_{3/2}$	0.43(3)	0.51(6)
$7S_{1/2} - 10P_{3/2}$	0.27(2)	0.18(2)
$7S_{1/2} - 11P_{3/2}$	0.19(1)	0.09(1)
$7S_{1/2} - 12P_{3/2}$	0.14(1)	0.05(1)
Tail		1.101(7)
Core		20(2)
vc		−1.0(5)
Total		316.6(2.4)
Others		317.8(2.4) [33]
		313.7 [50]
		325.8 [51]

[a]Values are taken from Ref. [52].

IV. RESULTS

A. C_3 coefficients of Fr atom

Previously, we calculated the C_3 coefficients for various material walls interacting with alkali atoms [37,41] except for Fr, so we are not repeating the results for other alkali atoms in the present work. Here, we provide the C_3 coefficients only for Fr with a number of material walls. We give the static $\alpha_d(0)$ value along with the reduced $E1$ matrix elements and their uncertainties for the Fr atom in Table I. Our $\alpha_d(0)$ value is also compared with the other high-precision calculations. We have taken the experimental values of $E1$ matrix elements of the dominant dipole transitions of Fr [52]. Other $E1$ matrix elements are calculated using the method given in Sec. III. Our value is in excellent agreement with value given by Derevianko *et al.*, who used high-precision experimental values for $E1$ matrix elements for the principal transitions and other

TABLE II. Calculated C_3 coefficients (in a.u.) of Fr with various material walls with explicit contributions from the core, vc, main, and tail parts of its dipole polarizability. The values in parentheses represent the estimated uncertainty.

	Core	vc	Main	Tail	Total
Au	0.899	−0.033	1.928	0.024	2.81(9)
Si	0.644	−0.025	1.643	0.020	2.28(6)
SiO_2	0.394	−0.014	0.776	0.010	1.17(4)
SiN_x	0.482	−0.019	1.173	0.011	1.65(5)
YAG	0.613	−0.023	1.130	0.014	1.73(6)
OS	0.658	−0.024	1.162	0.015	1.81(7)
ES	0.698	−0.029	1.167	0.015	1.85(7)

$E1$ values found with the SD method [33]. The value given by Safronova *et al.* is evaluated using the SD method and deviates from our value by around 1% [50]. Although the method we use is that same as that of Refs. [33,50] to calculate the dipole polarizability of Fr, we have also scaled the $E1$ matrix elements using experimental energies as explained in Sec. III. Recently, Śmiałkowski and Tomza used a molecular MOLPRO package to evaluate the dipole polarizability of Fr, which is overestimated and diverges by ∼3% from our value [51]. Using reduced $E1$ matrix elements given in Table I, we estimated the dynamic $\alpha_d(\iota\omega)$ values and then used them to estimate different contributions to C_3, as given in Table II. The dominant contributor of C_3 coefficients is the main part, followed by the core, tail, and vc. The total value of C_3 coefficient differs from material to material. Consequently, the various contributions have been added up to provide a final value of the C_3 coefficient. The core provides 27%–38% of the share of the total value of C_3, which is in agreement with the work by Derevianko *et al.* [33], who emphasized the sensitivity of the core to dipole C_3 values. On the other hand, the tail contribution is ∼1% of the total value. The uncertainty of the final value of C_3 comes entirely from the evaluation of dynamic dipole polarizabilities.

B. Quadrupole polarizabilities

To evaluate the C_5 coefficients, we require quadrupole polarizability of alkali atoms. In Table III, we present the static values of quadrupole polarizability $\alpha_q(0)$ of the ground states of alkali-metal atoms and compare our resulted values with the available literature. We calculated the static polarizability by putting $\omega = 0$ in Eq. (12). Since $E2$ matrix elements are required to calculate dynamic polarizability, we provide the matrix elements of the dominant $E2$ transitions in Table III for all the alkali atoms, and their uncertainties are quoted in the parentheses. The breakdown of polarizability into the main, tail, core, and vc polarizabilities is also presented. The main part of the valence polarizability provides the dominant contribution, followed by tail and core polarizabilities. The vc contributions for Li, Na, and K are zero due to the non-availability of D orbitals in the core of these atoms, whereas very insignificant contributions have been encountered for Rb, Cs, and Fr. For the final value of total static polarizability, we have added the core polarizability values from RPA. We have assigned percentage errors of 3%, 5%, 65%, 65%, 5%, and 15% to the tail part of α_q in Li, Na, K, Rb, Cs, and Fr, respectively. The net uncertainty of the corresponding final value of α_q is given by adding all the uncertainties in quadrature. From Table III, we can observe that with an increase in atomic number, the static quadrupole polarizabilities of alkali atoms from Li to Cs increase, but the trend breaks at Cs. It is expected that being the heaviest atom among all the alkalis, Fr could have the largest polarizability value. Even the previous studies on the dipole polarizability of alkali atoms report a higher $\alpha_d(0)$ value for the Cs atom than for Fr. The reason can be understood by looking into the various contributions to quadrupole polarizabilities in Table III. As can be seen, the principally contributing $E2$ matrix elements gradually increase with the size of an alkali atom, while the trend deviates from Cs to Fr. Since excitation energies of these transitions become larger with the size of the alkali atom, with similar $E2$ amplitudes, contributions from these principal transitions to quadrupole polarizabilities become lower. Also, the trends of "tail" contributions show a similar behavior from Cs to Fr, suggesting that $E2$ matrix elements of the higher excited states behave in a similar manner. The reason for lower magnitudes in the $E2$ matrix elements in Fr compared to Cs could be attributed to large cancellations in the electron correlation effects and strong relativistic effects in Fr due to the presence of more occupied electrons, including in the d orbitals. We did not find experimental $\alpha_q(0)$ results for any alkali atom to compare our theoretical values to. However, in Table III, we compare our results with the most recent work by Śmiałkowski *et al.*, who calculated the static quadrupole polarizability of alkali atoms using the MOLPRO package of *ab initio* programs [51]. Our static value for quadrupole polarizability deviates from the values reported by Śmiałkowski *et al.* by less than 1% for Li to Cs alkali atoms, whereas for Fr, the discrepancy is about 8%. In another work [19], Jiang *et al.* evaluated the dynamic quadrupole polarizability of Na and Cs using the oscillator method. We believe that our values are much more reliable than the comparable ones due to accurate calculations of the matrix elements evaluated using the AO method.

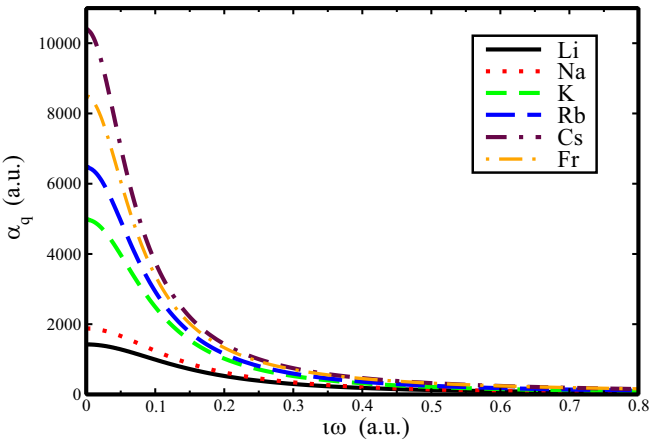

FIG. 1. Calculated dynamic quadrupole polarizability α_q (in a.u.) at imaginary frequencies of the alkali atoms.

Using the $E2$ matrix elements, the dynamic quadrupole polarizability $\alpha_q(\iota\omega)$ of alkali atoms over a range of frequencies was calculated as presented in Fig. 1. Since our static

TABLE III. Contributions to the ground-state quadrupole polarizabilities (in a.u.) of the Li, Na, K, Rb, Cs, and Fr atoms. Various contributions along with the $E2$ matrix elements contributing to the main part of the valence correlations are quoted explicitly. Tail, core, and valence-core contributions are also given. The RPA value of core has been considered for the total static value of α_q. Uncertainties in matrix elements and polarizability contributions are quoted in parentheses. Final results are compared with previously available values.

	Li			Na			K	
Contribution	$E2$	$\alpha_q(0)$	Contribution	$E2$	$\alpha_q(0)$	Contribution	$E2$	$\alpha_q(0)$
Main			Main			Main		
$2S_{1/2}-3D_{3/2}$	17.340(3)	421.9(1)	$3S_{1/2}-3D_{3/2}$	19.79(1)	589(1)	$4S_{1/2}-3D_{3/2}$	30.51(38)	1897(47)
$2S_{1/2}-4D_{3/2}$	7.282(1)	63.56(2)	$3S_{1/2}-4D_{3/2}$	7.783(3)	76.96(6)	$4S_{1/2}-4D_{3/2}$	4.32(87)	30(12)
$2S_{1/2}-5D_{3/2}$	4.303(2)	20.78(2)	$3S_{1/2}-5D_{3/2}$	4.465(2)	23.63(2)	$4S_{1/2}-5D_{3/2}$	0.69(66)	1(1)
$2S_{1/2}-6D_{3/2}$	2.957(1)	9.49(1)	$3S_{1/2}-6D_{3/2}$	3.020(1)	10.43(1)	$4S_{1/2}-6D_{3/2}$	0.13(47)	0.02(18)
$2S_{1/2}-7D_{3/2}$	2.208(1)	5.188(5)	$3S_{1/2}-7D_{3/2}$	2.234	6	$4S_{1/2}-7D_{3/2}$	0.35(34)	0.2(3)
$2S_{1/2}-8D_{3/2}$	1.734(2)	3.160(7)	$3S_{1/2}-8D_{3/2}$	1.80(5)	3.6(2)	$4S_{1/2}-8D_{3/2}$	0.40(28)	0.2(3)
$2S_{1/2}-3D_{5/2}$	21.24(60)	632(35)	$3S_{1/2}-3D_{5/2}$	24.23(2)	884(1)	$4S_{1/2}-3D_{5/2}$	37.36(46)	2846(70)
$2S_{1/2}-4D_{5/2}$	8.919(2)	95.34(4)	$3S_{1/2}-4D_{5/2}$	9.532(4)	115.4(1)	$4S_{1/2}-4D_{3/2}$	5.28(1.06)	44(18)
$2S_{1/2}-5D_{5/2}$	5.27(36)	31(4)	$3S_{1/2}-5D_{5/2}$	5.469(2)	35.45(3)	$4S_{1/2}-5D_{5/2}$	0.84(79)	1(2)
$2S_{1/2}-6D_{5/2}$	3.622(2)	14.24(2)	$3S_{1/2}-6D_{5/2}$	3.699(1)	15.64(1)	$4S_{1/2}-6D_{5/2}$	0.17(58)	0.04(27)
$2S_{1/2}-7D_{5/2}$	2.704(1)	7.781(6)	$3S_{1/2}-7D_{5/2}$	2.736(1)	8.38(1)	$4S_{1/2}-7D_{5/2}$	0.43(43)	0.2(5)
$2S_{1/2}-8D_{5/2}$	2.123(3)	4.74(1)	$3S_{1/2}-8D_{5/2}$	2.21(7)	5.4(3)	$4S_{1/2}-8D_{5/2}$	0.49(34)	0.3(4)
Tail		114(3)	Tail		104(8)	Tail		98(64)
Core		0.112(5)	Core		1.59(2)	Core		16(1)
vc		0	vc		0	vc		0
Total		1424(35)	Total		1880(5)	Total		4934(107)
Others		1423 [51]	Others		1895 [51]	Others		4962 [51]
					1800 [19]			

	Rb			Cs			Fr	
Contribution	$E2$	$\alpha_q(0)$	Contribution	$E2$	$\alpha_q(0)$	Contribution	$E2$	$\alpha_q(0)$
Main			Main			Main		
$5S_{1/2}-4D_{3/2}$	32.88(74)	2451(111)	$6S_{1/2}-5D_{3/2}$	33.62(2.07)	3422(420)	$7S_{1/2}-6D_{3/2}$	33.40(1.82)	3016(328)
$5S_{1/2}-5D_{3/2}$	0.09(92)	0.02(28)	$6S_{1/2}-6D_{3/2}$	12.97(41)	327(21)	$7S_{1/2}-7D_{3/2}$	8.47(39)	130(12)
$5S_{1/2}-6D_{3/2}$	2.10(45)	6(3)	$6S_{1/2}-7D_{3/2}$	8.08(17)	109(5)	$7S_{1/2}-8D_{3/2}$	5.94(15)	56(3)
$5S_{1/2}-7D_{3/2}$	2.00(26)	6(2)	$6S_{1/2}-8D_{3/2}$	5.54(9)	48(2)	$7S_{1/2}-9D_{3/2}$	4.26(39)	27(5)
$5S_{1/2}-8D_{3/2}$	1.71(17)	4(1)	$6S_{1/2}-9D_{3/2}$	4.11(7)	25(1)	$7S_{1/2}-10D_{3/2}$	3.23(6)	15.1(6)
$5S_{1/2}-9D_{3/2}$	1.44(12)	2.8(5)	$6S_{1/2}-10D_{3/2}$	3.21(3)	15.4(3)	$7S_{1/2}-11D_{3/2}$	2.57(5)	9.3(3)
$5S_{1/2}-4D_{5/2}$	40.29(90)	3681(164)	$6S_{1/2}-5D_{5/2}$	41.56(2.41)	5195(601)	$7S_{1/2}-6D_{5/2}$	41.54(2.02)	4610(449)
$5S_{1/2}-5D_{5/2}$	0.07(1.07)	0.01(24)	$6S_{1/2}-6D_{5/2}$	15.20(45)	448(27)	$7S_{1/2}-7D_{5/2}$	9.11(38)	150(12)
$5S_{1/2}-6D_{5/2}$	2.54(30)	9(4)	$6S_{1/2}-7D_{5/2}$	9.63(2)	156(6)	$7S_{1/2}-8D_{5/2}$	6.68(17)	71(4)
$5S_{1/2}-7D_{5/2}$	2.43(30)	9(2)	$6S_{1/2}-8D_{5/2}$	6.63(12)	69(2)	$7S_{1/2}-9D_{3/2}$	4.86(11)	35(2)
$5S_{1/2}-8D_{5/2}$	2.09(18)	6(1)	$6S_{1/2}-9D_{3/2}$	4.94(7)	37(1)	$7S_{1/2}-10D_{5/2}$	3.71(9)	20(1)
$5S_{1/2}-9D_{3/2}$	1.74(14)	4.2(6)	$6S_{1/2}-10D_{5/2}$	3.87(8)	22.3(9)	$7S_{1/2}-11D_{5/2}$	2.96(8)	12.4(6)
Tail		224(145)	Tail		644(32)	Tail		478(72)
Core		35(2)	Core		86(7)	Core		125(10)
vc		∼0	vc		∼0	vc		∼0
Total		6440(246)	Total		10606(736)	Total		8756(560)
Others		6485 [51]	Others		10498 [51]	Others		9225 [51]
					10600 [19]			

values are accurate, we believe that the dynamic values are also reliable. We find the static RPA and DF values for the core contributions are quite close, so we have estimated the dynamic values of core polarizabilities using the DF method without losing much accuracy. As the frequency increases, the polarizability value decreases and reaches a small value beyond $\omega = 1$ a.u. This trend is seen for every atom considered in the present work. Since these dynamic polarizability values can be important for experimental purposes, we have inferred these values at a particular frequency by providing a fitting model. In our previous work [53], we gave the fitting formula for the dipole polarizability of alkali atoms at imaginary frequencies. Here, we have fitted the quadrupole polarizabilities of all the alkali atoms using the following fitting formula:

$$\alpha_q(\iota\omega) = \frac{A}{1 + B\omega + C^2\omega}, \tag{21}$$

where A, Bm and C are the fitting parameter given in Table IV.

C. C_5 dispersion coefficients

Table V presents the calculated dispersion coefficients for all considered atoms due to the C_5 contributions of the

TABLE IV. Fitting parameters for the dynamic quadrupole polarizabilities of the alkali-metal atoms at imaginary frequencies.

	Atom					
Parameter	Li	Na	K	Rb	Cs	Fr
A	1425.04	1879.5	4980.82	6470.66	10420.9	8514.71
B	0.1296	0.1193	0.2097	0.3640	1.1656	0.9549
C	42.0983	49.7813	97.0513	115.692	163.194	138.994

TABLE V. Tabulated C_5 coefficients for the alkali-metal atoms with different material walls. The uncertainties in the final values are given in parentheses. Final results are compared with previously available theoretical values.

	Li						
	Au	Si	SiO_2	SiN_x	YAG	OS	ES
Core	0.001	0.004	0.003	0.003	0.005	0.005	0.006
vc	0	0	0	0	0	0	0
Main	17.657	14.870	7.292	10.808	10.827	11.181	11.320
Tail	2.046	1.694	0.861	1.243	1.288	1.338	1.365
Total	19.7(5)	8.1(4)	16.6(2)	12.1(2)	12.1(3)	12.5(3)	12.7(3)
Ref. [15]	19.15						
	Na						
	Au	Si	SiO_2	SiN_x	YAG	OS	ES
Core	0.077	0.048	0.034	0.036	0.054	0.059	0.064
vc	0	0	0	0	0	0	0
Main	22.610	19.081	9.308	13.846	13.801	14.242	14.401
Tail	1.762	1.464	0.738	1.072	1.103	1.144	1.165
Total	24.45(9)	20.59(8)	10.08(4)	14.95(6)	14.96(6)	15.44(6)	15.63(6)
Ref. [19]	25.2						
Ref. [15]	22.48						
	K						
	Au	Si	SiO_2	SiN_x	YAG	OS	ES
Core	0.702	0.465	0.308	0.347	0.486	0.530	0.571
vc	0	0	0	0	0	0	0
Main	47.036	39.962	19.117	28.784	28.151	28.972	29.146
Tail	1.873	1.539	0.792	1.132	1.188	1.236	1.264
Total	50(1)	42(1)	20.2(6)	30.3(9)	29.8(9)	31(1)	31(1)
Ref. [15]	47.48						
	Rb						
	Au	Si	SiO_2	SiN_x	YAG	OS	ES
Core	1.435	0.973	0.631	0.728	0.992	1.076	1.154
vc	~ 0	~ 0	~ 0	~ 0	~ 0	~ 0	~ 0
Main	55.231	46.980	22.377	33.765	32.876	33.818	33.973
Tail	3.743	3.106	1.569	2.274	2.345	2.433	2.479
Total	60(3)	51(2)	25(1)	37(2)	36(2)	37(2)	38(2)
	Cs						
	Au	Si	SiO_2	SiN_x	YAG	OS	ES
Core	3.277	2.287	1.442	1.712	2.252	2.431	2.591
vc	~ 0	~ 0	~ 0	~ 0	~ 0	~ 0	~ 0
Main	73.938	62.855	29.809	45.015	43.596	44.834	44.941
Tail	9.070	7.605	3.761	5.538	5.594	5.785	5.867
Total	86(5)	73(4)	35(2)	52(3)	51(3)	53(3)	53(3)
Ref. [19]	117						
	Fr						
	Au	Si	SiO_2	SiN_x	YAG	OS	ES
Core	4.418	3.126	1.943	2.341	3.026	3.257	3.462
vc	~ 0	~ 0	~ 0	~ 0	~ 0	~ 0	~ 0
Main	64.978	55.310	26.252	39.656	38.457	39.548	39.669
Tail	7.169	5.987	2.985	4.369	4.448	4.606	4.680
Total	77(4)	64(4)	31(2)	46(3)	46(3)	47(3)	48(3)

polarizability in the total potential interacting with different material walls. Using the resulting dynamic polarizability of the considered atoms and dynamic permittivity values of material walls at imaginary frequencies, we obtained the C_5 vdW dispersion coefficients using Eq. (7). The estimated uncertainties of the final values are quoted in parentheses. We have used an exponential grid to solve the integration of the mentioned equation. In Table V, core, vc, main, and tail contributions of dispersion coefficients are given which are explicitly based on the corresponding contribution of polarizability. The final value of the C_5 coefficient was found by adding up all the contributions. The increasing size of the alkali atoms increases the values of the individual contribution and total dispersion coefficients due to the increasing polarizability of the atom for any particular material wall. Among the various contributions, the main part is the dominant contributor to the total C_5 dispersion coefficient value, followed by the tail, core, and vc. In Ref. [33], Derevianko *et al.* emphasized that the C_3 coefficients are sensitive to the core contribution. However, for the case of the C_5 coefficients, the core C_5 coefficients are much smaller and contribute at most 5% to total C_5 value, whereas the tail C_5 contributions are prominent. The zero value of the vc contribution of the C_5 coefficient for Li, Na, and K is due to the zero value of the quadrupole polarizability. After comparing the presented C_5 coefficients with the C_3 coefficients that were already reported in our previous work [37,41], it can be observed that C_3 values are at least 25 times smaller than C_5 values for any particular system. The reason for this difference solely depends on the larger quadrupole polarizability of alkali atoms compared to their dipole polarizability. Moreover, the Fr atom has lower values of final C_5 coefficients than Cs due to the smaller valence quadrupole polarizability of Fr than Cs. Comparing the materials considered in the present work, the largest C_5 values are observed for metal (Au), followed by the semiconductor (Si) and then dielectrics (sapphire, YAG, SiN_x, and SiO_2).

We also compare our values with the available theoretical values of C_5 coefficients. Jiang *et al.* reported C_5 coefficients for Na and Cs with different materials, including Au [19]. The reported value for the Na-Au system is in close agreement with our value. But for the case of the Cs-Au system, our value deviates from the reported value by 35%. The reason for the discrepancies could be the method used for the calculation of the dynamic polarizability and permittivity of the atom and material, respectively. The oscillator method has been used to calculate the quadrupole polarizability of Na and Cs. This method overestimates the polarizability values, especially when the systems become heavier [54]. It can also be seen from Table V that $\alpha_d(0)$ for Cs is not reliable. This could be one of the reasons for the overestimated value of the C_5 coefficient reported by Jiang *et al.* The dynamic polarizability values of Na and Cs of Jiang *et al.* were evaluated using the oscillator method, which gave results that deviate slightly from our values, whereas the dynamic permittivity of Au was evaluated using a single-frequency Lorentzian approximation, as a result of which the C_5 coefficients reported by them are exaggerated. In another report, Tao and Rappe calculated the C_5 coefficients for Li, Na, and K with Au using an *ab initio* DFT + vdW method [15]. Although our values support the values reported in Ref. [15], the deviation of our values from the reported ones starts increasing with the increase in the size of the atom. As it is commonly known that the exchange-correlation functional and nonlocal correlation energies are not treated properly in the DFT method, we believe our values are accurate and more reliable than the values given by Tao *et al.*

D. Total vdW potentials

The primary findings of the present work are given in this section. Figure 2 presents the potential curves due to dipole and quadrupole effects evaluated using Eqs. (2) and (3), respectively, for alkali-metal atoms interacting with the SiN_x system. Most of the experiments have been conducted with SiN_x diffraction grating [40,55–61], so for demonstration purposes, we have chosen a SiN_x wall to observe the total potential curves with alkali atoms. The total potential curve has been obtained to the first higher-order interaction of the atom-wall system within the framework of Lifshitz theory. The individual dipole and quadrupole potential curves are also plotted. We have evaluated U_d using our previous value of dipole polarizability [37,41]. It can be observed that the quadrupole contribution makes a very small contribution to the total potential. If we scrutinize these graphs at very short separation distances, i.e., from $z = 1$ to $z = 10$ a.u., as presented in the insets in Figs. 2(a)–2(f), we can observe the overwhelming contribution provided by the quadrupole contribution of the atom-wall potential. The quadrupole contribution is more dominant than the dipole from 1 to 6 nm for all the alkali-metal atoms. As the separation distance increases, the long-range dispersion interaction is completely imparted by the dipole effect of the polarizability of the atom as depicted in Fig. 2. These results suggest that for a particular material the quadrupole effects can be quite significant if the separation distance is very small. Also, the quadrupole effect is much more effective and can be realized over a larger separation when the atom or molecule considered is profoundly polarized. Similar curves can be obtained for the other materials that have been considered in this work. It can be conjectured that the higher-order contributions after the quadrupole term might influence the total vdW potential in the preliminary test. This might be true at the diminutive separation distance between the atom and a wall, but the Lifshitz theory is not applicable below a separation distance of 1 nm [62]. Earlier studies on physisorption of an atom on materials have shown that octupole contributions give corrections of about 0.5%–1% to the total vdW potentials of different atom-surface interactions [63–65]. Hence, we neglect higher-order contributions and restrict the potentials until quadrupole polarization effects.

V. CONCLUSION

We have investigated the quadrupole polarization effects of alkali atoms in the total atom-wall van der Waals interaction potentials. For this, we considered both dipole- and quadrupole-induced interactions of atoms with

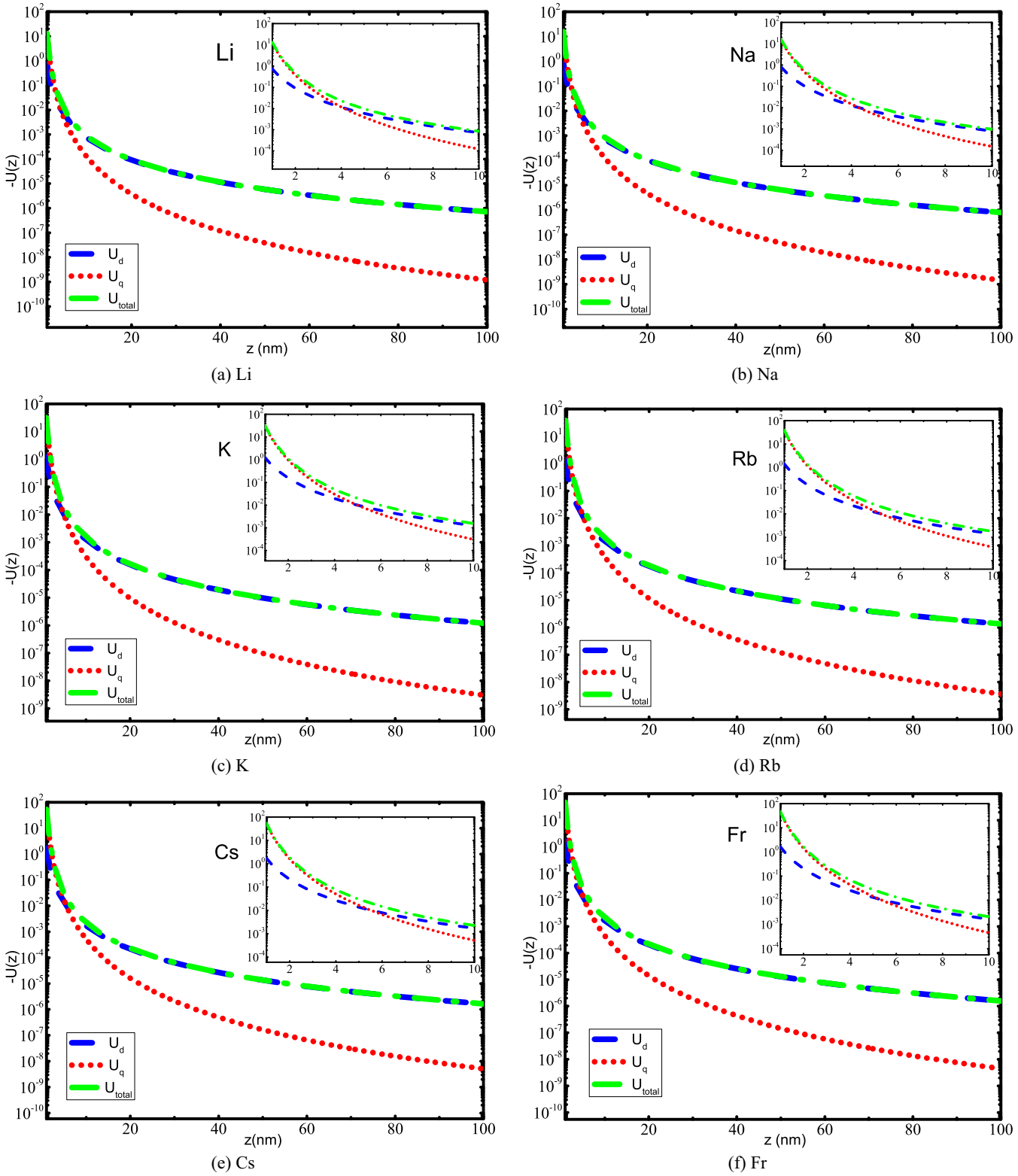

(a) Li (b) Na (c) K (d) Rb (e) Cs (f) Fr

FIG. 2. The vdW potential curves for interactions of the alkali-metal atoms with SiN_x for $z = 1$–100 nm. The insets present the same potential curves at $z = 1$–10 nm.

various material walls within the framework of Lifshitz theory. We probed the range of the separation distance at which these quadrupole effects are dominant. The potential curves depict that the quadrupole polarization effects of alkali atoms in a total atom-wall potential are quite significant when the separation distance between the atom and material wall ranges from 1 to 10 nm. Beyond this range, the quadrupole contributions start declining, resulting in an attractive potential entirely due to the dipole polarization effects. Also, at significantly shorter distances, the

attraction due to quadrupole polarization of the alkali atom increases with the increase in the size of the atom, suggesting quadrupole effects can be dominant when an atom has a greater tendency to be polarized. The obtained results could be useful in high-precision experiments for studying van der Waals interactions at smaller distances very close to surfaces.

ACKNOWLEDGMENTS

Research at the Perimeter Institute is supported in part by the government of Canada through the Department of Innovation, Science and Economic Development and by the province of Ontario through the Ministry of Colleges and Universities.

[1] M. Antezza, L. P. Pitaevskii, and S. Stringari, Phys. Rev. A **70**, 053619 (2004).
[2] G. G. Kleiman and U. Landman, Phys. Rev. B **8**, 5484 (1973).
[3] H. Kaur, N. Shukla, R. Srivastava, and B. Arora, Phys. Rev. A **104**, 012806 (2021).
[4] E. V. Blagov, G. L. Klimchitskaya, and V. M. Mostepanenko, Phys. Rev. B **71**, 235401 (2005).
[5] V. Bhojawala and D. Vakharia, Microsyst. Technol. **23**, 1255 (2017).
[6] V. B. Bezerra, G. L. Klimchitskaya, V. M. Mostepanenko, and C. Romero, Phys. Rev. A **78**, 042901 (2008).
[7] A. Derevianko, B. Obreshkov, and V. A. Dzuba, Phys. Rev. Lett. **103**, 133201 (2009).
[8] R. Folman, P. Krüger, D. Cassettari, B. Hessmo, T. Maier, and J. Schmiedmayer, Phys. Rev. Lett. **84**, 4749 (2000).
[9] T. Peyrot, N. Šibalić, Y. R. P. Sortais, A. Browaeys, A. Sargsyan, D. Sarkisyan, I. G. Hughes, and C. S. Adams, Phys. Rev. A **100**, 022503 (2019).
[10] M. Bordag, G. L. Klimchitskaya, U. Mohideen, and V. M. Mostepanenko, *International Series of Monographs on Physics* Vol. 145 (Oxford University Press, Oxford, 2009).
[11] E. Lifshitz and M. Hamermesh, in *Perspectives in Theoretical Physics*, edited by L. Pitaevski (Pergamon, Amsterdam, 1992), pp. 329–349.
[12] A. Dalgarno and G. A. Victor, Proc. Phys. Soc. **90**, 605 (1967).
[13] A. Liebsch, Phys. Rev. B **35**, 9030 (1987).
[14] V. V. Klimov and M. Ducloy, Phys. Rev. A **62**, 043818 (2000).
[15] J. Tao and A. M. Rappe, Phys. Rev. Lett. **112**, 106101 (2014).
[16] J. Tao, J. P. Perdew, and A. Ruzsinszky, Phys. Rev. B **81**, 233102 (2010).
[17] J. Tao and A. M. Rappe, J. Chem. Phys. **144**, 031102 (2016).
[18] E. R. Johnson and A. D. Becke, J. Chem. Phys. **124**, 174104 (2006).
[19] X.-P. Jiang, F. Toigo, and M. W. Cole, Surf. Sci. **145**, 281 (1984).
[20] J. M. Hutson, P. Fowler, and E. Zaremba, Surf. Sci. Lett. **175**, L775 (1986).
[21] G. Łach, M. DeKieviet, and U. D. Jentschura, Phys. Rev. A **81**, 052507 (2010).
[22] A. Sargsyan, T. Vartanyan, and D. Sarkisyan, Opt. Spectrosc. **128**, 575 (2020).
[23] A. Laliotis, B.-S. Lu, M. Ducloy, and D. Wilkowski, AVS Quantum Sci. **3**, 043501 (2021).
[24] M. Sun, W. Tang, Q. Ren, S. Wang, J. Yu, Y. Du, and Y. Zhang, Appl. Surf. Sci. **356**, 668 (2015).
[25] K. A. Whittaker, J. Keaveney, I. G. Hughes, A. Sargsyan, D. Sarkisyan, and C. S. Adams, Phys. Rev. A **92**, 052706 (2015).
[26] G. Gwinner and L. Orozco, Quantum Sci. Technol. **7**, 024001 (2022).
[27] K. Harada, T. Aoki, K. Kato, H. Kawamura, T. Inoue, T. Aoki, A. Uchiyama, K. Sakamoto, S. Ito, M. Itoh, T. Hayamizu, A. Hatakeyama, K. Hatanaka, T. Wakasa, Y. Sakemi *et al.*, J. Phys.: Conf. Ser. **691**, 012017 (2016).
[28] E. Gomez, L. A. Orozco, and G. D. Sprouse, Rep. Prog. Phys. **69**, 79 (2006).
[29] S. Aubin, E. Gomez, L. Orozco, and G. Sprouse (unpublished).
[30] Y. Sakemi, K. Harada, M. Itoh, S. Ito, A. Uchiyama, T. Inoue, H. Kawamura, T. Aoki, A. Hatakeyama, Y. Takahashi, J. Hisano *et al.*, *Fundamental Physics with Cooled Radioactive Atoms* (JPS Conference Proceedings, Kanazawa, Japan, 2021), p. 011016.
[31] S. Sanguinetti, R. Calabrese, L. Corradi, A. Dainelli, A. Khanbekyan, E. Mariotti, C. de Mauro, P. Minguzzi, L. Moi, G. Stancari, L. Tomassetti, S. Veronesi *et al.*, Opt. Lett. **34**, 893 (2009).
[32] J. Grond, U. Hohenester, I. Mazets, and J. Schmiedmayer, New J. Phys. **12**, 065036 (2010).
[33] A. Derevianko, W. R. Johnson, M. S. Safronova, and J. F. Babb, Phys. Rev. Lett. **82**, 3589 (1999).
[34] M. K. Öztürk and S. Özçelik, arXiv:physics/0406027.
[35] E. M. Lifshitz, Sov. Phys. JETP **2**, 73 (1956).
[36] G. Łach, M. DeKieviet, and U. D. Jentschura, Int. J. Mod. Phys. A **25**, 2337 (2010).
[37] B. Arora and B. K. Sahoo, Phys. Rev. A **89**, 022511 (2014).
[38] E. D. Palik, *Handbook of Optical Constants of Solids* (Academic, San Diego, 1998), Vol. 3.
[39] G. L. Klimchitskaya, U. Mohideen, and V. M. Mostepanenko, Phys. Rev. A **61**, 062107 (2000).
[40] J. D. Perreault, A. D. Cronin, and T. A. Savas, Phys. Rev. A **71**, 053612 (2005).
[41] K. Kaur, J. Kaur, B. Sahoo, and B. Arora, Phys. Lett. A **380**, 3366 (2016).
[42] J. Kaur, D. K. Nandy, B. Arora, and B. K. Sahoo, Phys. Rev. A **91**, 012705 (2015).
[43] Y. Singh and B. K. Sahoo, Phys. Rev. A **90**, 022511 (2014).
[44] M. S. Safronova, W. R. Johnson, and A. Derevianko, Phys. Rev. A **60**, 4476 (1999).
[45] S. A. Blundell, W. R. Johnson, Z. W. Liu, and J. Sapirstein, Phys. Rev. A **40**, 2233 (1989).
[46] A. Kramida, Y. Ralchenko, J. Reader, and NIST ASD Team, NIST Atomic Spectra Database, version 5.8, `https://physics.nist.gov/asd`.
[47] H. Kaur, S. Singh, B. Arora, and B. K. Sahoo, Phys. Rev. A **105**, 032819 (2022).
[48] M. S. Safronova, and U. I. Safronova, Phys. Rev. A **85**, 022504 (2012).
[49] M. S. Safronova and U. I. Safronova, Phys. Rev. A **83**, 052508 (2011).

[50] U. I. Safronova, W. R. Johnson, and M. S. Safronova, Phys. Rev. A **76**, 042504 (2007).
[51] M. Śmiałkowski and M. Tomza, Phys. Rev. A **103**, 022802 (2021).
[52] J. E. Simsarian, L. A. Orozco, G. D. Sprouse, and W. Z. Zhao, Phys. Rev. A **57**, 2448 (1998).
[53] S. Dutt, S. Singh, A. Mahajan, B. Arora, and B. Sahoo, Phys. Scr. **95**, 095506 (2020).
[54] B. Arora, H. Kaur, and B. K. Sahoo, J. Phys. B **47**, 155002 (2014).
[55] A. D. Cronin and J. D. Perreault, Phys. Rev. A **70**, 043607 (2004).
[56] J. D. Perreault and A. D. Cronin, Phys. Rev. A **73**, 033610 (2006).
[57] S. Lepoutre, V. Lonij, H. Jelassi, G. Trénec, M. Büchner, A. Cronin, and J. Vigué, Eur. Phys. J. D **62**, 309 (2011).
[58] V. P. A. Lonij, W. F. Holmgren, and A. D. Cronin, Phys. Rev. A **80**, 062904 (2009).
[59] J. D. Perreault and A. D. Cronin, Phys. Rev. Lett. **95**, 133201 (2005).
[60] V. P. A. Lonij, C. E. Klauss, W. F. Holmgren, and A. D. Cronin, Phys. Rev. Lett. **105**, 233202 (2010).
[61] R. E. Grisenti, W. Schöllkopf, J. P. Toennies, G. C. Hegerfeldt, and T. Köhler, Phys. Rev. Lett. **83**, 1755 (1999).
[62] D. Bloch and M. Ducloy, Adv. At., Mol., Opt. Phys. **50**, 91 (2005).
[63] C. Holmberg and P. Apell, Phys. Rev. B **30**, 5721 (1984).
[64] P. Apell and C. Holmberg, Solid State Commun. **49**, 1059 (1984).
[65] C. Holmberg and P. Apell, Solid State Commun. **49**, 513 (1984).